Energy Proceedings
Vol 49, 2024
ISSN 2004-2965

Analysis operational characteristics and potential faults of PEMFC in PEMFC - battery powered bulldozers#

Yang Xiaomei [1], Tan Piqiang [1]*, Liu Xiaoyang [1], Tian Congfeng [1,2], Lou Diming [1], Hu Zhiyuan [1]

1 School of Automobile Studies, Tongji University, Shanghai, 201804, China

2. Shantui Construction Machinery Co., Ltd., Shandong, 272073, China
(tanpq@hotmail.com)

ABSTRACT

Research on Proton exchange membrane fuel cell (PEMFC) bulldozers is currently in its infancy. Performing crucial investgation of fuel cell operation characteristics and potential faults based on the bulldozer operating conditions is beneficial for the promotion of fuel cell applications. In this work, with a 110 kW PEMFC and a 90 kW battery used as the power system for the bulldozer. The contents are threefold. Firstly, a numerical model integrating the bulldozer, cabin, motor and power system is established, and the accuracy and reliability of the model is evaluated. After that, based on the operating conditions of bulldozer including no-load, soil-cutting, soil-transportation and unloading soil stage, the operation characteristics of the fuel cell system are analyzed. To detailed analyze the variation patterns of the various parameters inside the fuel cell under the aforementioned operating conditions, a three-dimensional numerical model of fuel cell is established. The results indicate that PEMFC power and current density rapidly increase to 110 kW and 1.513 A/cm² during the soil-cutting phase, and then decrease rapidly to 50 kW and 0.551 A/cm² during the unloading soil phase, showing significant rate of change. The PEMFC stack temperature can reach a maximum of 346 K. The average liquid saturation in gas diffusion layer reaches a maximum of 0.30 at the end of the soil-transport phase, and the uneven distribution of internal liquid is significant. There is significant uneven distribution of liquid, which could lead to localized flooding issues at the end of soil-transport. Appropriate strategies need to be implemented to control.

Keywords: Proton exchange membrane fuel cell (PEMFC), Potential faults, Bulldozer, construction machinery, Typical operating conditions

NONMENCLATURE

b	Track wheel width, m
c	Soil cohesion coefficient
C_{H2}、C_{O2}	H_2, O_2 concentrations at the anode and cathode membranes, mol/cm^3
C_{st}	Specific heat capacity, J/(kg·K)
E	Theoretical electrode potential, V
F	Faraday constant, 96 485 C/mol
F_{br}	Bulldozing resistance, N
F_{cr}	Climbing resistance, N
F_i	Internal friction resistance, N
F_{roll}	Rolling resistance, N
$\triangle G$	Gibbs free energy, J/mol
J_{max}	Actual current density, A/cm^2
k	Rolling resistance coefficient
K_{pc}, K_p	Coefficient related to soil bearing friction angle
M	Weight of bulldozer, kg
M_{st}	Stack mass, kg
P_{H2}, P_{O2}, P_{H2O}	Partial pressure of H2, O2, H2O, atm
Q_{tot}	Reaction chemical energy, J
Q_{cl}	cooling heat dissipation, J
Q_g	gas flow heat dissipation, J
Q_{st}	energy output, J
R	Gas constant, 8.314 J/(mol·K)
r	Unit volume of soil, N/m3
R_{ohm}	Equivalent resistance, Ω
T	Actual temperature, K
U_{act}	Activation polarization, J
U_{ohm}	Ohmic polarization, J
U_{conf}	Concentration polarization, J
z	Track subsidence, m
γ	Internal friction coefficient
Θ	Slope angle, °
ε_1, ε_2, ε_3, ε_4, ε_5	Experience coefficient

1. INTRODUCTION

As the world's dedication to environmental stewardship deepens, there is an escalating urgency for

This is a paper for the 16th International Conference on Applied Energy (ICAE2024), Sep. 1-5, 2024, Niigata, Japan.

the transition of heavy machinery industries, which have long relied on fossil fuels. Proton exchange membrane fuel cell technology provides a new power solution for the heavy machinery industry with advantages such as zero emissions, high efficiency, and compatibility with renewable energy. However, bulldozers operate under harsh working conditions, with frequent and significant changes in fuel cell power, resulting in weak stability and low reliability of bulldozer fuel cells [4].

The unstable operation of fuel cell systems may lead to malfunctions. Variations in load can alter the reaction intensity within PEMFC stacks, potentially leading to malfunctions like flooding, membrane dehydration, hydrogen starvation, and catalyst decay [5,6]. A fault, if not promptly detected and addressed, can disrupt the PEMFC system's stable operation. A fault, if not promptly detected and addressed, can disrupt the PEMFC system's stable operation. In severe cases, it may lead to irreversible damage to the fuel cell stack or result in completing shutdown [7]. Therefore, the stable operation of PEMFC stacks is the key to the stable operation of the entire system. Zhang et al. [8] studied the effects of operating parameters such as back pressure, relative humidity, and stoichiometric ratio on the PEMFC performance through experiments, and demonstrated the uniformity and stability of PEMFC performance using polarization curves, electrochemical impedance spectroscopy, and segmented cell technology. The research results indicate that higher back pressure can improve the overall performance of PEMFC, and an increase in relative humidity can enhance the local performance, current distribution uniformity, and local stability of fuel cells. Meng et al. [9] studied the voltage response characteristics of PEMFC under different degrees of hydrogen and oxygen deficiency through experiments. The results show that in the absence of hydrogen, the response voltage exhibits a parabolic trend, which has a significant impact, and raising the working temperature can effectively alleviate the fault phenomenon. Both experiments and numerical simulations can reflect the PEMFC performance. The results show that a hydrogen vehicle with a degraded fuel cell consumes 14.3% more fuel than a fresh fuel cell hydrogen vehicle. At present, fuel cell bulldozers are still in the research stage. Real time monitoring of bulldozer fuel cells under bulldozer operating conditions is being carried out to clarify the operating characteristics of fuel cells under bulldozer operating conditions, which is conducive to achieving a more stable and reliable operating mode for fuel cell bulldozers.

At present, PEMFC bulldozers are currently in its infancy. Real time monitoring of bulldozer fuel cells under bulldozer operating conditions is being carried out to clarify the operating characteristics of fuel cells under bulldozer operating conditions, which is conducive to achieving a more stable and reliable operating mode for fuel cell bulldozers.

Therefore, this work established a one-dimensional (1D) simulation model of the PEMFC-battery bulldozer and a three-dimensional (3D) PEMFC model, and conducted reliability verification. Monitor the parameters of PEMFC-battery bulldozer under typical operating conditions, analyze the characteristics of electrical, reactant, temperature, liquid water and other parameters. This investigation into the effects of bulldozer operating conditions on PEMFC performance and potential faults is crucial for advancing the reliable application of PEMFC in construction machinery.

2. NUMERICAL MODEL

2.1 Physical model

The schematic of PEMFC-battery bulldozer structure is shown in Fig.1. The bulldozer is driven by two motors, and its power is provided by a PEMFC with a rated power of 110 kW and a battery with a rated power of 90 kW. The electronic control unit (ECU) determines the output power of the PEMFC and battery based on the different operating states of the bulldozer. The power is provided by the battery when the motor's power demand is too low, and by the fuel cell when the motor's power demand is high. When the required power of the motor is greater than the rated power of the PEMFC, the excess power is provided by the battery. The basic parameters of fuel cell bulldozers can be found in Table 1.

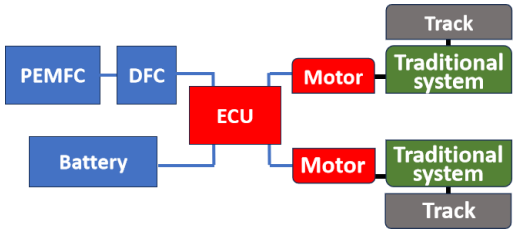

Fig. 1 Schematic of PEMFC-battery bulldozer structure

Table 1 Parameters of PEMFC-battery *bulldozer [11]*

Component	Parameters	Quantity
PEMFC	Rated power/kW	110
bettery	Rated power/kW	90
Motor	maximum power/kW	105
	maximum torque/Nm	800
	rated speed/rpm	1430
Bulldozer	curb weight/kg	28000
	track width/m	0.61

track length/m	3.05
drive wheel radius/m	0.46831

2.2 Numerical model

(1) Bulldozer operation

The resistance during the operation of bulldozers includes rolling resistance, bulldozing resistance, climbing resistance and traditional internal friction resistance [12]

Rolling resistance:

$$F_{roll}=k\cdot M \tag{1}$$

Bulldozing resistance:

$$F_{br}=b\cdot(c\cdot z\cdot K_{pc}+0.5\cdot z^2\cdot r\cdot K_{pr}) \tag{2}$$

Climbing resistance:

$$F_{cr}=W\cdot sin(\Theta) \tag{3}$$

Traditional internal friction resistance:

$$F_i=\gamma\cdot W \tag{4}$$

(2) PEMFC [13,14]

The basic reaction of PEMFC stack: total reaction $H_2(g)+0.5O_2(g)\rightarrow H_2O(g)$. The reaction occurring on the anode side is $H_2\rightarrow 2H^++2e^-$, and the generated electrons reach the cathode side through an external circuit. H+reaches the cathode through a proton exchange membrane and reacts with oxygen at the cathode to produce water. The reaction occurring on the cathode side is $O_2+4H^++4e^-\rightarrow 2H_2O$. Electrons move directionally in an external circuit to generate current.

Theoretical electrode potential of PEMFC:

$$E=-\frac{\Delta G}{2F}+\frac{RT}{2F}\left[\ln\left(P_{H_2}\right)+\frac{1}{2}\ln\left(P_{O_2}\right)-\ln\left(P_{H_2O}\right)\right] \tag{5}$$

However, the PEMFC stack is affected by the reaction rate, internal resistance, and differences in reactant gas concentration, leading to activation polarization, ohmic polarization, and concentration polarization losses.

$$U_{act}=\varepsilon_1+\varepsilon_2 T\ln C_{H_2}+\varepsilon_3 T\ln C_{O_2}+\varepsilon_4 T\ln I \tag{6}$$

$$U_{ohm}=IR_{ohm} \tag{7}$$

$$U_{con}=-\varepsilon_5\ln\left(1-\frac{J}{J_{max}}\right) \tag{8}$$

(3) PEMFC temperature [16]:

$$\frac{dT_{st}}{dt}=\frac{Q_{tot}-Q_{cl}-Q_g-Q_{st}}{C_{st}M_{st}} \tag{9}$$

2.3 Model validation

To verify the accuracy of the simulation model of the fuel cell bulldozer, the model was validated. Fig. 2 and Fig. 3 present the comparison results between the model simulation results and the experimental results. Fig. 2 clearly shows that the speed error of the model is within 1.0% and the power error is within 5.0%, compared with the experimental data [11]. According to Fig. 3, the polarization curve, power density and stack temperature errors of PEMFC are all within 6.5%, comparing the experimental data of references [15] and [16].

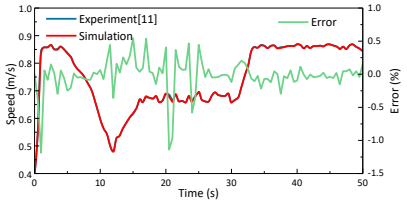

(a) Speed

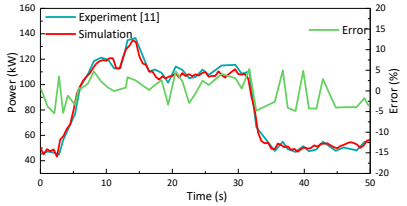

(b) Power

Fig. 2 Comparison between simulation results and experiments of bulldozer [11]

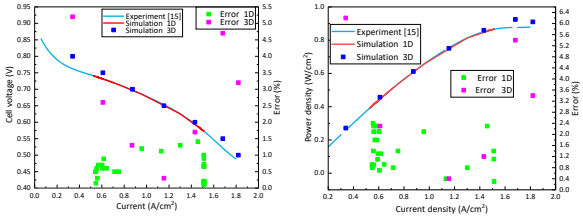

(a) Polarization curve *(b) Power density*

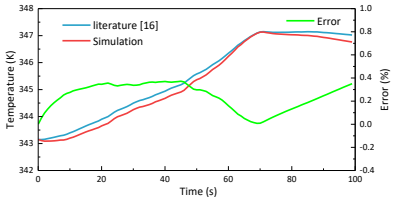

(c) Stack temperature

Fig. 3 Comparison between simulated and experimental values of PEMFC[15, 16]

3. RESULTS AND DISCUSSION

The typical operating conditions of bulldozers include five operating states: 1-4 seconds of no-load, 4-16 seconds of soil-cutting, 16-31 seconds of soil-transportation, 31-33 seconds of unloading soil and 33-50 seconds of no-load stage. Before operating this condition, the operating temperature of the fuel cell was 343.15 K, and the bulldozer was moving at a speed of 0.4 m/s with a slope of 0.

3.1 Electrical monitoring

Fig. 4 depicts the variation in battery power under typical operating conditions of bulldozers. It can be observed that the power required by the motor shows an initial increase followed by a slight decrease, and fluctuations around a certain power level. Subsequently, there is a rapid decrease in power followed by

fluctuations around another power level. The motor power is approximately 45 kW during 0-4 s. From 4-14 s, the power rapidly increases to a maximum of about 135 kW. Between 15-18 s, the power decreases and fluctuates around 106 kW. The power rapidly decreases and fluctuates around 50 kW between 31 - 33 s. The main reasons are as follows: the bulldozer is in a no-load state during 0-4 s, experiencing fluctuating road conditions and speed variations, resulting in motor power fluctuating around 50 kW. The bulldozer is engaged in soil-cutting state from 4-16 s, reaching maximum digging depth at the 14 s, which increases digging resistance, and thus demands maximum motor power. The bulldozer is transporting soil during 16-31 s, requiring steady high power around 106 kW. The bulldozer is unloading soil state during 31-33 s, rapidly reducing the load and causing a swift decrease in power. From 33-50 s, it returns to a no-load stage with lower power demand, fluctuating around 50 kW due to minor terrain variations and speed changes.

The power demanded by the motor is primarily supplied by the PEMFC. When the motor power demand is below 105 kW, the PEMFC provides all the power. If the motor power demand exceeds 105 kW, the excess power is supplied by the battery. This is primarily because when the motor power exceeds 105 kW, there are fluctuations in power demand. To minimize PEMFC fluctuations, the ECU controls the fluctuating power by having the battery handle it, thereby ensuring stable operation of the PEMFC.

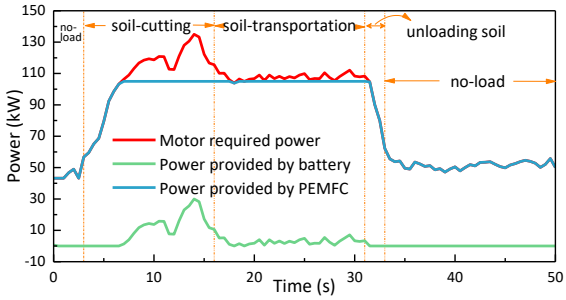

Fig.4 The variation of battery power under typical operating conditions

Fig. 5 illustrates the variations in PEMFC power distribution, current density, State of charge (SOC), PEMFC and cell voltage under typical operating conditions. It can be observed from Fig. 5(a) that a lot of operational power of the PEMFC is provided to the motor, and a small portion used to charge the battery. Additionally, the SOC gradually decreases during both the soil-cutting and soil-transportation stages. At the 8 s, the PEMFC reaches power of 110 kW, with 105 kW supplied to the motor and 5 kW used for charging the battery. From Fig. 5(b), it is noted that the trend of PEMFC current density aligns closely with the power trend, peaking at 1.513 A/cm2 during the soil-cutting and soil-transportation stages, and dropping to approximately 0.551 A/cm2 during no-load periods. Conversely, the trend in cell voltage shows an inverse relationship with current density, reaching a minimum of 0.573 V during soil-cutting and soil-transportation stages, and approximately 0.738 V during no-load periods.

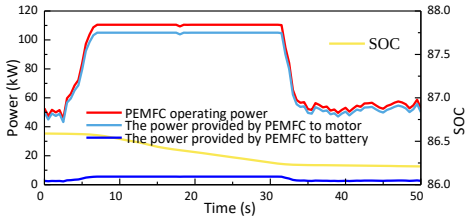

(a) PEMFC power allocation and SOC variation

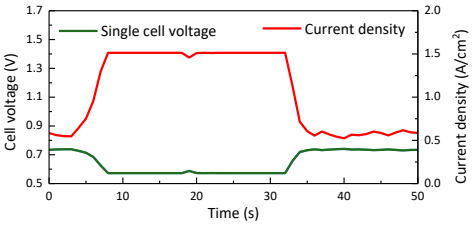

(b) Trend of PEMFC current density and cell voltage variation

Fig. 5: Changes in PEMFC power distribution, current density, SOC and cell voltage under typical operating conditions

3.2 Reactant monitoring

Fig. 6 shows the variation trend of inlet gas mass flow to the stack under typical operating conditions. It can be observed that the inlet mass flow at both the cathode and anode exhibits minor fluctuations before 4 s, increases after 4 s, and reaches maximum values around 8 s. Subsequently, there are minor fluctuations around this point, with a rapid decrease in mass flow around 31 s reaching a minimum value at approximately 35 s, fluctuating around this value thereafter. The mass flow at the cathode and anode fluctuates around 43.0 g/s and 1.5 g/s during the no-load stage, respectively. Due to rapid power demand increase during the soil-cutting state, the mass flow at the cathode and anode quickly increases to approximately 115.52 g/s and 2.56 g/s. Due to rapid power demand decrease in the unloading soil stage, the mass flow decreases rapidly to around 43.0 g/s and 1.5 g/s respectively, fluctuating around these values. This is mainly because there is a rapid increase and decrease in motor power demand during the soil-cutting and soil-transportation stages. The power demand is relatively stable during the soil-transportation and no-

load stages, resulting in smaller variations of reactant mass.

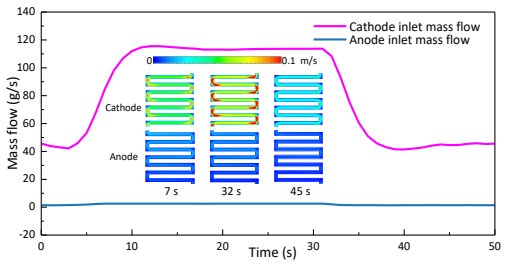

Fig. 6 Variations in inlet gases of the Stack under typical operating conditions

3.3 Temperature monitoring

Fig. 7 depicts the variation in stack and coolant temperatures under typical operating conditions. It is observed that the stack temperature, cathode/anode outlet temperatures, coolant inlet/outlet temperatures, and cathode inlet temperature exhibit a trend of gradual increase followed by a slow decrease over time. The cathode/anode outlet temperatures align closely with the stack temperature, starting at approximately 345 K, gradually increasing to about 349 K, and then slowly decreasing back to around 345 K. The maximum coolant inlet temperature is about 340 K, and the outlet temperature reaches of 346 K. This is primarily due to the higher power demand and stronger chemical reactions during the PEMFC soil-cutting and soil-transportation stages, resulting in more heat generation, whereas less heat is generated during no-load periods with lower power requirements.

The cathode inlet temperature shows significant variation during the soil-cutting and soil-transportation stages, increasing from 335 K to 344 K and then decreasing to around 335 K. This is because during the soil-cutting stage, there is a substantial increase in air flow rate, leading to higher operational power of the air compressor and consequently more heat generation. Afterward, the temperature reduction is minimal as the air passes through the intercooler. Subsequently, the air enters the humidifier where the temperature of the humidified exhaust air is also high, resulting in a higher cathode inlet temperature.

Additionally, Fig. 7 illustrates that the trend in anode inlet temperature is opposite to that of the cathode. During the soil-cutting phase, the temperature decreases from 294 K to 281 K and then increases to 294 K during the unloading soil stage. This is primarily reason that the anode is primarily heated and humidified by the hydrogen circulation pump. And during the soil-transportation stage, an increase in hydrogen mass flow rate leads to a decrease in the temperature of the incoming gas mixed with the circulated gas from the hydrogen circulation pump.

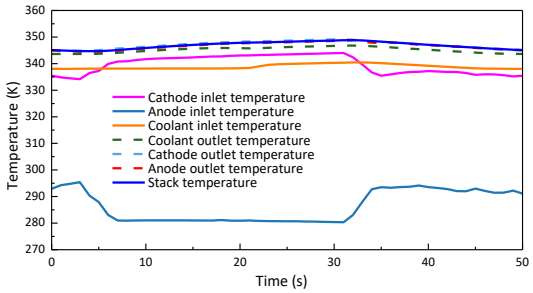

Fig. 7 Variations in stack and coolant temperatures under typical operating conditions.

3.4 Liquid water monitoring

Fig. 8 shows the variation trend of liquid saturation in the PEMFC at different operating times of the bulldozer. Fig. 8(a) depicts the trend of liquid saturation in catalyst layer. It is observed that the liquid saturation rapidly increases during the soil-cutting stage, gradually stabilizes during the soil-transportation stage, sharply decreases during the unloading soil stage, and eventually stabilizes during the no-laod stage. The maximum average liquid water saturation reaches 0.18 at the 32 s and stabilizes at 0.13 after unloading soil. Fig. 8 (b) shows the liquid saturation in gas diffusion layer, the average liquid saturation reaching a maximum of 0.30 at the 32 s. The main reason is that from the soil-cutting stage, current density rapidly increases, maintains a higher value during pushing stage, and decreases during the unloading soil phase. This leads to corresponding changes in the water generated by the reactions. Fig. 8 also indicate uneven distribution of liquid, with less at the gas inlet side and more at the outlet side, especially pronounced at the 32 s. This unevenness is primarily due to gas flow carrying away some liquid, gradually accumulating at the outlet side. The water produced during the soil-transportation phase gradually accumulates, reaching its maximum at the 32 s. This causes uneven distribution of liquid in the 32 s. This phenomenon increases the likelihood of localized flooding towards the end of the pushing stage and the beginning of the dumping stage.

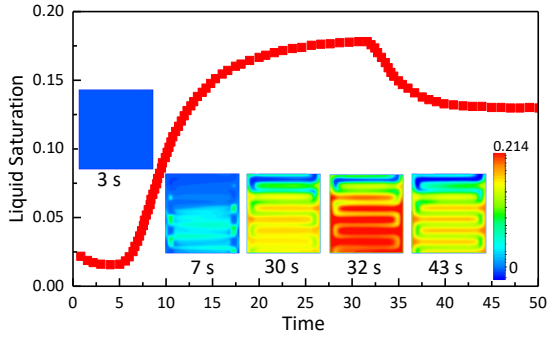

(a) Liquid saturation of catalytic layer

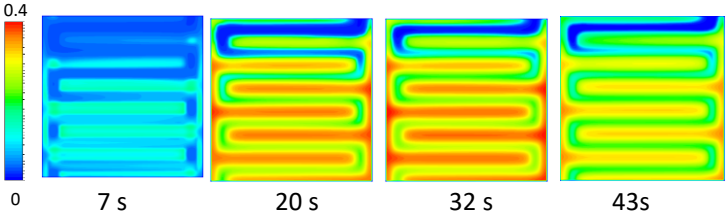

(b) Liquid saturation of microporous layer

Fig. 8: liquid saturation of cathode

4. CONCLUSIONS

This work establishes a simulation model for a PEMFC-battery powered bulldozer, analyzing the variation trends in PEMFC performance under typical operating conditions. The aim is to clarify the stability of PEMFC operation and potential failure points during bulldozer operations. These findings provide insights into optimizing PEMFC performance and operational stability in PEMFC-battery bulldozers applications. The main conclusions are as follows:

(1) PEMFC power and current density rapidly increase to 110 kW and 1.513 A/cm² during the soil-cutting phase, and then decrease rapidly to 50 kW and 0.551 A/cm² during the unloading soil phase, showing significant rate of change.

(2) The PEMFC stack temperature can reach a maximum of 346 K. The average liquid saturation in gas diffusion layer reaches a maximum of 0.30 at the end of the soil-transport phase. The uneven distribution of internal liquid is significant.

(3) There is significant uneven distribution of liquid, which could lead to localized flooding issues at the end of soil-transport. Appropriate strategies need to be implemented to control.

ACKNOWLEDGEMENT

This work was supported by Key R&D Program of Shandong Province, China (No. 2023CXGC010210).

REFERENCE

[1] Habip S. Hydrogen refueling of a fuel cell electric vehicle. INT J HYDROGEN ENERG 2024; 75: 604-612.

[2] He XY, Jiang Y. Review of hybrid electric systems for construction machinery. AUTOMAT CONSTR 2018; 92: 286-296.

[3] Li KR, Hong JC, Zhang C, et al. Health state monitoring and predicting of proton exchange membrane fuel cells: A review. J POWER SOURCES 2024; 612: 234828.

[4] Lin C, Yan XH, Wei GH, et al. Optimization of configurations and cathode operating parameters on liquid-cooled proton exchange membrane fuel cell stacks by orthogonal method. APPL ENERG 2019; 253: 113496.

[5] Byungwoo K, Wonbin N, Hyeongcheol L. Model-Based Fault Analysis and Diagnosis of PEM Fuel Cell Control System. APPLIED SCIENCES 2022; 12(24): 12733-12733.

[6] Wang J, Yang B, Zeng C, et al. Recent advances and summarization of fault diagnosis techniques for proton exchange membrane fuel cell systems: A critical overview. J POWER SOURCES 2021; 500: 229932.

[7] Ren P, Pei P, Li Y, et al. Diagnosis of water failures in proton exchange membrane fuel cell with zero-phase ohmic resistance and fixed-low-frequency impedance. APPL ENERG 2019; 239, 785-792.

[8] Zhang G, Yuan H, Wang Y, et al. Three-dimensional simulation of a new cooling strategy for proton exchange membrane fuel cell stack using a non-isothermal multiphase model. APPL ENERG 2019; 255: 113865.1-113865.10.

[9] Meng K, Chen B, Zhou H, et al. Experimental investigation on voltage response characteristics of hydrogen-oxygen proton exchange membrane fuel cells under gas starvation. ENERG CONVERS MANAGE 2022; 268, 115973.

[10] Ahmadi P, Khoshnevisan A. Dynamic simulation and lifecycle assessment of hydrogen fuel cell electric vehicles considering various hydrogen production methods. INT J HYDROGEN ENERG 2022; 47(62): 26758-26769.

[11] Wang H, Huang YJ, Khajepour A, et al. A novel energy management for hybrid off-road vehicles without future driving cycles as a priori. Energy 2017; 133: 929-940.

[12] Zhu XN, Pan LY, Sun ZZ, et al. Simulation tool for dozer data acquisition. AUTOMAT CONSTR 2022; 142: 104522.

[13] Mousavi SB, Ahmadi P, Raeesi M. Performance evaluation of a hybrid hydrogen fuel cell/battery bus with fuel cell degradation and battery aging. RENEW ENERG 2024; 227: 120456.

[14] ZHAO Yang, WANG Shubo, LI Weiwei, XIE Xiaofeng. Polarization of the membrane electrode assembly in a proton exchange membrane fuel cell. Journal of Tsinghua University (Science and Technology) 2020; 60(3): 254-262.

[15] Lu JB, Shen XM, Chen M, et al. Synergistic effect of cathode humidity and current density on performance of PEMFC. CHINESE JOURNAL OF POWER SOURCES 2021; 45(8): 1018-1022.

[16] Ma Y, Hu FY, Hu YF. Energy efficiency improvement of intelligent fuel cell/battery hybrid vehicles through an integrated management strategy. ENERGY 2023; 263(E): 125794.